IEEE Access
Multidisciplinary | Rapid Review | Open Access Journal

Received 9 February 2023, accepted 22 February 2023, date of publication 27 February 2023, date of current version 2 March 2023.

Digital Object Identifier 10.1109/ACCESS.2023.3249662

APPLIED RESEARCH

Estimation of Number of Cores for Preventing Common-Mode Inductor Saturation in Railway Traction Inverters

SATORU HATSUKADE[1,2], (Member, IEEE), AND KEIJI WADA[2], (Senior Member, IEEE)
[1]Vehicle Technology Division, Railway Technical Research Institute, Kokubunji, Tokyo 185-8540, Japan
[2]Graduate Schools of Systems Design, Tokyo Metropolitan University, Hachioji, Tokyo 192-0397, Japan
Corresponding author: Satoru Hatsukade (hatsukade@mem.iee.or.jp)

ABSTRACT In the traction system of rolling stock, the common-mode (CM) voltage is over 500 V, so the inductors that suppress the CM current are prone to saturation. To prevent saturation, the traction inverter needs many numbers of cores inside CM inductors, but the required number of cores has been determined empirically. This paper proposes a method calculate the approximate number of nanocrystalline cores to avoid saturation of CM inductors in railway traction inverters without circuit simulation. Using the only the CM capacitance of traction motor and the core characteristics on the datasheet, the maximum flux density of the inductor is calculated. Comparing calculated results of the maximum flux density with the results measured with a 1500 V DC inverter indicates that the proposed method can better identify the occurrence of saturation than the methods based on CM current presented in the literature. Furthermore, for the entire CM voltage range from 500 V to 3000 V, the minimum number of cores which saturation is prevented by the proposed calculation method is shown to be in reasonable agreement with the simulation results.

INDEX TERMS Electromagnetic interference, inductors, inverters, magnetic cores.

I. INTRODUCTION

In traction inverters for rolling stock, the reduction of electromagnetic interference (EMI) is particular importance [1], [2], [3], [4], [5]. Various measures are required to comply with the limitations of international standards such as IEC 62236 series (European standards are EN 50121 series) and requirements such as EN 50238 series for electromagnetic radiation from different railway signaling systems [6], [7]. Common-mode (CM) currents must be suppressed to reduce radiation from traction inverters. Filters consisting of CM inductors have been widely studied not only in rolling stock [8], [9], [10], [11], [12], [13], [14], [15], [16], [17]. Since traction inverters in rolling stock have a large normal operating current, motor cables are bundled together and penetrating through many toroidal-shaped magnetic cores to form a CM inductor [16], [17]. For these magnetic cores, nanocrystalline with highly saturated magnetic flux density and high permeability are the best choice. However, since the CM voltage exceeds 500 V in the traction inverters, the inductors must be carefully designed to avoid saturation.

The magnetic flux density in the magnetic core of a CM inductor can be calculated either by integrating the applied voltage waveform or by calculating of the CM current [17], [18], [19]. However, if the high-frequency characteristics of magnetic materials are ignored, an excessive magnetic material size will be required in railway vehicles. In addition, since the CM impedance of the motor is unknown at the design stage, the number of cores to be equipped inside the traction inverter is designed empirically. Methods for designing core size based on the slope of CM voltage [16] and various high-frequency models of magnetic materials [20], [21], [22], [23], [24], [25], [26] are the methods that consider the high-frequency characteristics of magnetic materials. However, these methods are effective only when the core material and shape can be freely designed or when the frequency characteristics of the core can be measured in advance. Generally, railway traction inverters are equipped with many commercially available cores, making it difficult to apply the results of above-mentioned studies.

The associate editor coordinating the review of this manuscript and approving it for publication was Pinjia Zhang.

Based on the core datasheet [27], circuit simulation including saturation is now possible. This presents challenges, such as the need to know the CM impedance of the motor. In addition, it is time consuming to repeat the circuit simulation many times to determine the number of cores.

This paper proposes a simple method for calculating the number of cores required to prevent saturation in the design of CM inductors with nanocrystalline cores for traction inverters in rolling stock, using spreadsheet tools like Microsoft EXCEL®without circuit simulation. First, this paper shows a simplified CM circuit using these cores and a formula for calculating the maximum magnetic flux density inside the cores. The only parameters needed for this calculation are only the datasheet of the core (AL value, saturation flux density, effective cross-sectional area, and frequency characteristics of complex permeability), the capacitance in the CM impedance of the motor, and CM voltage of the traction. In other words, the calculation can be performed without the actual motor, inverter, and core. Next, from the measurement results using a 1500V DC traction inverter and the simulation results (reproducing the measurement results), the proposed maximum magnetic flux density calculation could properly determine the presence or absence of saturation under six test conditions with different numbers of cores and windings. Furthermore, we confirmed the superiority of the proposed method with respect to the number of cores required to avoid saturation. The proposed method agrees well with the simulation results, whereas the conventional method is more than twice as large as the simulation results.

II. CALCULATION OF MAXIMUM FLUX DENSITY IN THE CORE OF THE CM INDUCTOR OF THE RAILWAY TRACTION INVERTER

A. PROPOSED METHOD

In actual magnetic materials, the effective permeability decreases at high frequencies. This phenomenon occurs because the magnetic field inside the core, which is composed of thin metallic films, is partially canceled by the eddy currents in the thin films [24].

If a model considers this magnetic field cancellation, the magnetic flux in the model can approach the actual magnetic flux inside the core. However, this paper aims to determine how many cores need to be installed to avoid saturation during the design phase of railway traction inverters. Therefore, the application user can obtain only the AL value, effective the cross-sectional area, and the frequency characteristics of the complex permeability of the magnetic material from the core datasheet. A following is a method for calculating the magnetic flux density using only these values is shown below.

Figure 1 shows the circuit model of a traction inverter and motor with CM inductors containing nanocrystalline cores. The CM circuit of the motor is assumed to have only capacitance C_m. The CM voltage V_com of the traction inverter is a step voltage. For further simplification, the equivalent circuit of the CM inductor is only the first stage of a Cauer I-type

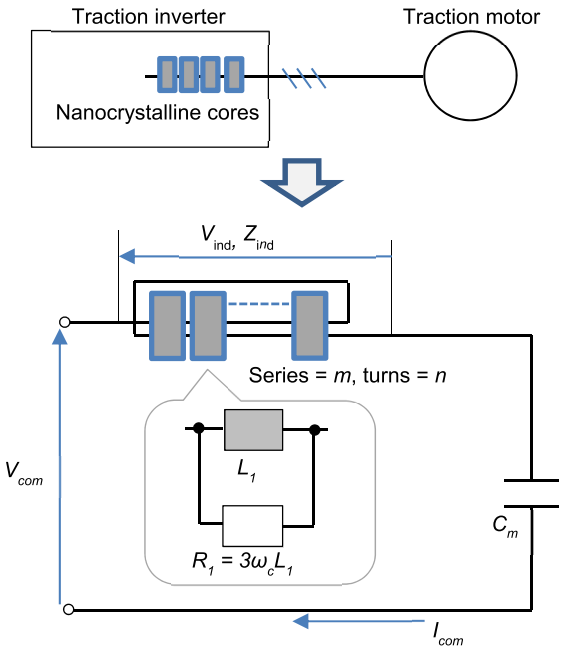

FIGURE 1. A common-mode circuit for a motor drive system considering core's high-frequency characteristics.

circuit [24], with L_1 as the single-core inductance component and R_1 as the resistance component. Since the CM inductor consists of multiple cores connected in series and wrapped around a motor cable, the CM equivalent impedance is n^2m times that of a single core.

The symbol ω_c in Fig. 1 is the cutoff frequency, which can be read from the characteristic graph of complex permeability [27]. In the case of Hitachi Metals Finemet®FT-3KM, which is widely used in rolling stock, ω_c is 6 kHz. When m cores are connected in series and the number of windings is n, the impedance Z_ind of the inductor is expressed by (1). In (1), the symbol s is the Laplace operator:

$$Z_\mathrm{ind} = n^2 m \frac{sL_1R_1}{sL_1 + R_1} \tag{1}$$

Since the applied CM voltage of the inductor corresponds to (2), the magnetic flux $\boldsymbol{\Phi}$ inside the inductor corresponds to (3).

$$V_\mathrm{ind} = \frac{V_\mathrm{com}}{s}\frac{Z_\mathrm{ind}}{Z_\mathrm{ind} + \frac{1}{sC_\mathrm{m}}} \tag{2}$$

$$\boldsymbol{\Phi} = \frac{V_\mathrm{ind}}{ns} = \frac{V_\mathrm{com}}{ns^2}\frac{Z_\mathrm{ind}}{Z_\mathrm{ind}+\frac{1}{sC_\mathrm{m}}} = \frac{V_\mathrm{com}}{s^2 + \frac{s}{n^2mC_\mathrm{m}R_1} + \frac{1}{n^2mL_1C_\mathrm{m}}} \tag{3}$$

By solving (3) for the oscillating state assuming zero initial flux (the damping and critical conditions are rare and can be ignored), time variation and maximum flux can be obtained by (4) and (5), respectively.

$$\boldsymbol{\Phi} = \frac{V_\mathrm{com}}{b}\mathrm{e}^{-at}\sin bt, a = \frac{1}{2n^2mC_\mathrm{m}R_1},$$
$$b = \sqrt{\frac{1}{n^2mL_1C_\mathrm{m}} - a^2} \tag{4}$$

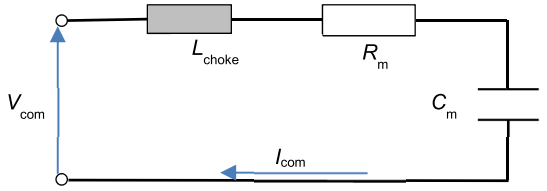

FIGURE 2. CM circuit of CM inductor and traction motor.

$$\Phi_{max} = \frac{V_{com}}{b} e^{-at_0} \sin bt_0,\ Ct_0 = \frac{1}{b} cos^{-1} \frac{a}{\sqrt{a^2+b^2}} \tag{5}$$

The maximum magnetic flux density per core, B_{max}, is (6).

$$B_{max} = \frac{V_{com}}{bmA_c} e^{-at_0} \sin bt_0 \tag{6}$$

B. PREVIOUS METHODS

To compare with the method proposed in the preceding section IIA, this paper presents some methods of calculating the magnetic flux in the CM inductors of earlier studies. In both studies, the magnetic flux in the CM inductor is calculated by multiplying the CM current by the inductance of the CM inductor. There is also a method [17] for calculating the CM current from the CM voltage through rate. However, since the calculation result of the maximum flux density is independent of the number of cores, this paper excludes it from comparisons.

1) CALCULATION FROM CM CURRENT

Figure 2 shows a CM circuit with a traction motor and a CM inductors. The symbol L_{ind} is the inductance of the CM inductor, and R_m is the resistance component of the CM circuit of the traction motor. Since Fig. 2 is an LCR series circuit, if the CM voltage is a step voltage, and the initial CM current is zero, the CM current I_{com} is given by (7) [18].

$$I_{com} = \frac{V_{com}}{\sqrt{1-\zeta^2}Z_0} e^{-\zeta\omega_n t} \sin\sqrt{1-\zeta^2}\omega_n t \tag{7}$$

where (8) shows each constant.

$$\omega_n = \frac{1}{\sqrt{L_{ind}C_m}},\ C\zeta = \frac{R_m}{2}\sqrt{\frac{C_m}{L_{ind}}},\quad CZ_0 = \sqrt{\frac{L_{ind}}{C_m}} \tag{8}$$

The time with maximum CM current is (9) by calculating the maximum value in the differentiation of (7) (there are multiple maximum values for t_1, but the minimum value after zero provides the maximum CM current).

$$t_1 = \frac{1}{b} cos^{-1} \frac{p}{\sqrt{p^2+q^2}},\quad Cp = \zeta\omega_n,\ Cq = \sqrt{1-\zeta^2}\omega_n \tag{9}$$

The maximum magnetic flux is expressed in (10).

$$\Phi_{max} = \frac{V_{com}L_{ind}}{\sqrt{1-\zeta^2}Z_0} e^{-\zeta\omega_n t_0} \sin\sqrt{1-\zeta^2}\omega_n t_1 \tag{10}$$

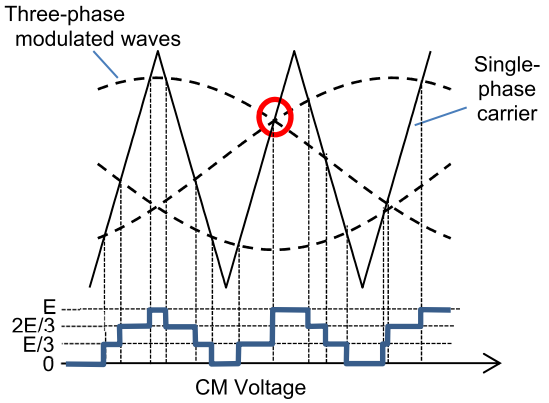

FIGURE 3. CM voltage generated by a single-phase carrier.

When $L_{ind} = n^2 mL_1$ in (10), we obtain B_{max} as (11).

$$B_{max} = \frac{V_{com}n^2L_1}{A_c\sqrt{1-\zeta^2}Z_0} e^{-\zeta\omega_n t_1} \sin\sqrt{1-\zeta^2}\omega_n t_1, \tag{11}$$

As an approximation to (11), (12) with $\zeta = 0$ is used in previous studies [17], [18].

$$I_{com\_max} \cong \frac{V_{com}}{Z_0} = V_{com}\sqrt{\frac{C_m}{L_{ind}}} \tag{12}$$

The flux maximum obtained from (12) is (13).

$$\Phi_{max} \cong \frac{V_{com}L_{ind}}{Z_0} = V_{com}\sqrt{L_{ind}C_m} \tag{13}$$

When m cores are connected in series and n is the number of windings, L_{ind} is $n^2 mL_1$. We can obtain the approximation (14) for the maximum flux density from (13).

$$B_{max} \cong \frac{V_{com}\sqrt{n^2mL_1C_m}}{mA_c} = \frac{V_{com}n\sqrt{L_1C_m}}{\sqrt{m}A_c} \tag{14}$$

2) CONDITION IN DUMPING

Ogasawara and Akagi [18] shows the method of damping the CM current by inserting a resistor R_d in the secondary side of a CM transformer. In this case, the CM current is (15), and the maximum value of the magnetic flux is (16).

$$I_{com} = \frac{V_{com}}{R_d} e^{-\frac{t}{C_m R_d}} \tag{15}$$

$$\Phi_{max} = \frac{V_{com}L_{ind}}{R_d} \tag{16}$$

According to (16), the maximum magnetic flux density in the core is (17), with L_1 as the inductance of a single core, A_c as the effective cross-sectional area, m as in the number of cores in series, and n as the number of windings.

$$B_{max} = \frac{V_{com}n^2mL_1}{mA_cR_d} = \frac{V_{com}n^2L_1}{A_cR_d} \tag{17}$$

In such circumstances, the damping resistance is the same as the internal resistance in Fig. 1. The maximum magnetic flux

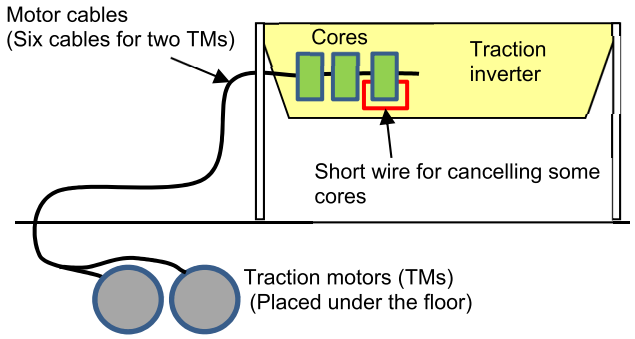

FIGURE 4. Test setup for verification testing of two parallel motor drives.

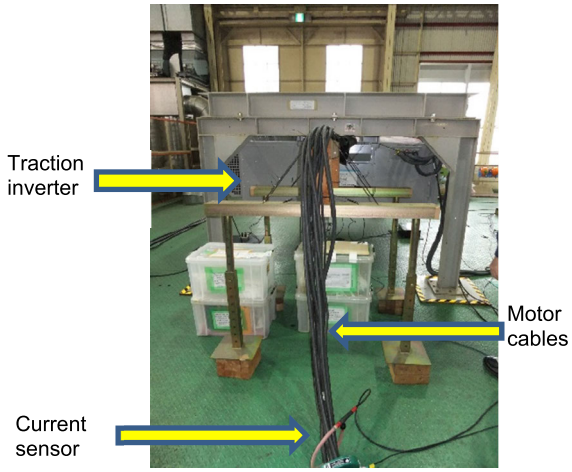

FIGURE 5. Photo of the test setup.

density can be obtained as (18) with $R_d = n^2 m R_1$.

$$B_{max} = \frac{V_{com} n^2 L_1}{A_c n^2 m R_1} = \frac{V_{com} L_1}{A_c m R_1} \tag{18}$$

C. CM VOLTAGE OF RAILWAY TRACTION INVERTER

Most railway traction inverters calculate switching timing by comparing a three-phase sine wave with a single-phase triangular wave. In the asynchronous mode shown in Fig. 3, there is timing when the triangular wave intersects two sine waves simultaneously. At this time, the two phases turn on and off simultaneously, and the CM voltage applied to the CM circuit is two-thirds of the DC input voltage E for the DC traction inverter, which is 1000 V if the DC catenary voltage is 1500 V. This is more likely to occur at low speeds and low modulation rates. As in many previous studies [28], [29], the CM voltage generated by a single switching is one-third of E in high-speed and synchronous mode.

Saturation due to CM voltage also depends on carrier frequency [30], [31]. The carrier frequency of traction inverters for rolling stock is about 500 Hz for GTOs and 2 kHz for IGBTs [32]. The UK Class 390 has a carrier frequency of 1.8 kHz [33]. In addition, Siemens AG is developing a traction inverter with a carrier frequency of 3 kHz using SiC [34]. On the other hand, if the harmonics of the carrier frequency exceed 10 kHz, they may match the frequency of signaling devices such as axle counter systems [35]. Therefore, a carrier frequency of 3 kHz is the current upper limit for traction inverters of rolling stock.

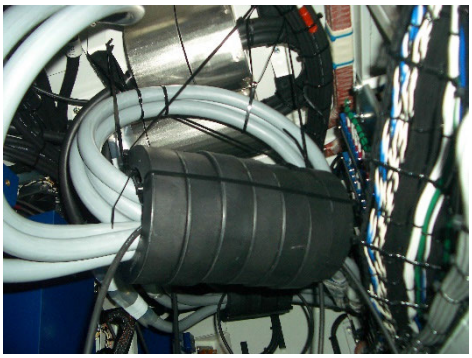

FIGURE 6. Cores inside traction inverter.

TABLE 1. Measurement cases.

Case	Series of Cores m	Turns n	Number of series cores with the same inductance
I	4	1	4
II	7	1	7
III	11	1	11
IV	14	1	14
V	4	2	16
VI	7	2	28

The time variation of the flux in the CM choke contains an exponential function as shown in (4) in section IIA. The time constant τ is given by (19).

$$\tau = 1/a = 2n^2 m C_m R_1 = 6n^2 m \omega_c C_m L_1 \tag{19}$$

If we assume $C_m = 36.1$ nF and $L_1 = 150$ μH as a realistic condition in section III, we obtain (20).

$$\tau = n^2 m \times 1.22 \times 10^{-6} [\mathrm{s}] \tag{20}$$

From (20), in the range $n^2 m < 135$, the time constant τ is sufficiently small relative to the half period of the carrier frequency of 3 kHz, and the magnetic flux is expected to decay to near zero before the next CM voltage change. Therefore, for the saturation of the CM choke in the traction inverter for rolling stock, it is sufficient to consider the CM voltage as two-thirds of the step voltage of the DC input voltage.

Note that when the modulation ratio is extremely low, the all three phases can be switched on or off simultaneously, because the values of the three-phase modulation waves are close together. In this case, it is sufficient to consider the CM voltage as a step voltage equal to the DC input voltage.

III. VERIFICATION WITH MEASUREMENT RESULTS

A. CM CURRENT MEASUREMENT IN TRACTION INVERTER

To verify the flux density calculation method presented in Section IIA, the CM current in a traction inverter with an input voltage of 1500 V DC was measured for a commuter train. The traction inverter drives two asynchronous traction motors in parallel. Figures 4 and 5 show the diagram and

TABLE 2. Simulation parameters.

	Parameter	Value
Core	AL value L_1	150 μH/n^2
	Cross sectional Area A_c	427.5 mm^2
	Cutoff frequency ω_c	6 kHz
	Saturation flux density B_{sat}	1.23 T
Motor	Resistance R_m	4.51 Ω
	Capacitance C_m	36.1 nF
	Inductance L_m	45.5 μH

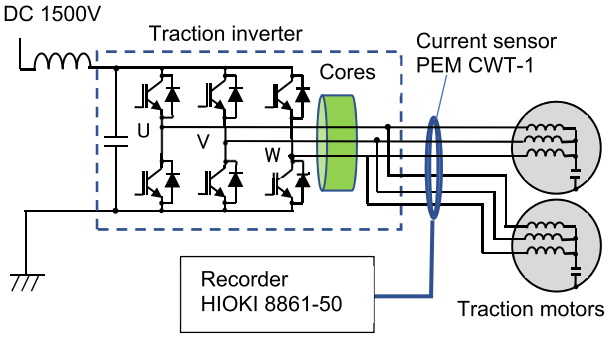

FIGURE 7. Test and measurement circuit.

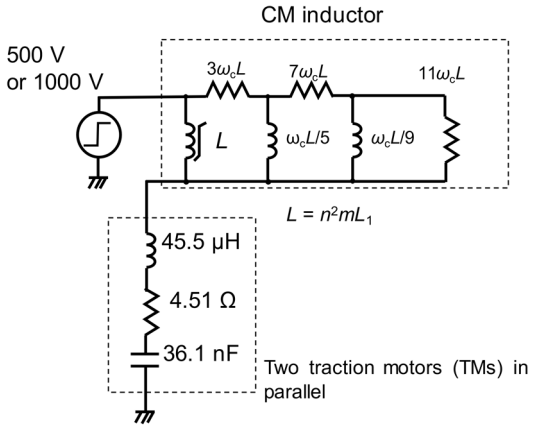

FIGURE 8. Simulation circuit.

the photograph of the test setup, respectively. The cores are installed inside (Fig. 6) and outside the inverter.

To reproduce the saturation of CM inductors, the number of cores connected in series and the number of turns in the windings varied. Table 1 shows the measurement cases. The cores used were FT-3KM F140100 (Hitachi Metals). Table 1 also shows the number of series of cores with the same inductance in each case. The individual cores are not identical across to save time when changing cases (As shown in Fig. 4, multiple cores were prepared, and each case was created by shortening unnecessary cores).

Figure 7 shows the setup for the CM current measurements. Since the traction inverter drives two traction motors in parallel, the CM current is measured as the sum of the two motors. Due to the configuration of this test, the CM current is recorded for approximately 1 second at the inverter startup.

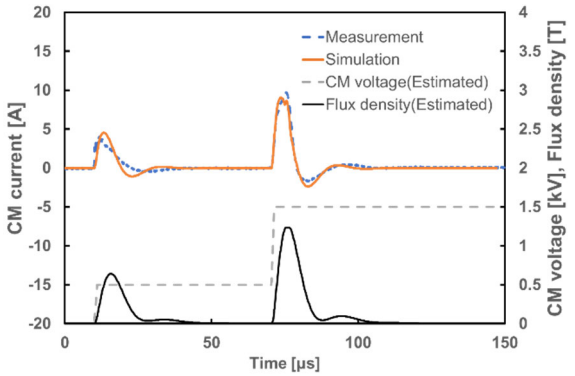

FIGURE 9. Measurement and simulation results (Case I).

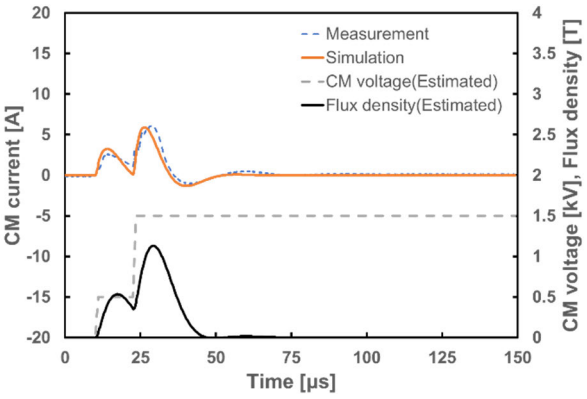

FIGURE 10. Measurement and simulation results (Case II).

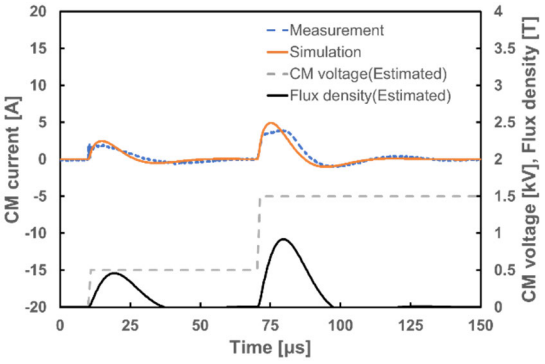

FIGURE 11. Measurement and simulation results (Case III).

This is due to the possibility of high CM voltage shown in Section IIC.

B. ESTIMATING FLUX DENSITY WITH CIRCUIT SIMULATION

Since the magnetic flux density was not measured in the measurement described in the previous section, circuit simulation was performed to estimate the magnetic flux density inside the core. The circuit simulation is based on the literature [27], confirming that the current waveform is close to the measured waveform.

Figure 8 shows the simulation circuit. Table 2 lists the parameters used in the simulations. AL values in the datasheet has range from 63 to 150 μH/n^2, so L_1 was fixed at

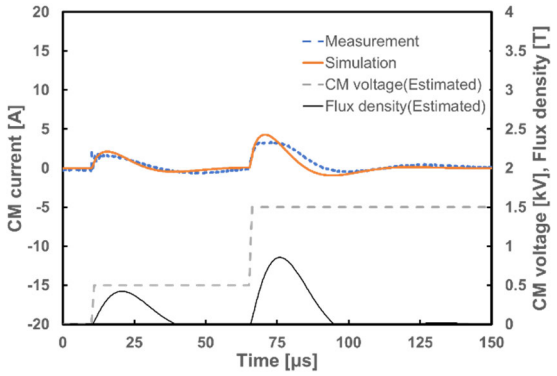

FIGURE 12. Measurement and simulation results (Case IV).

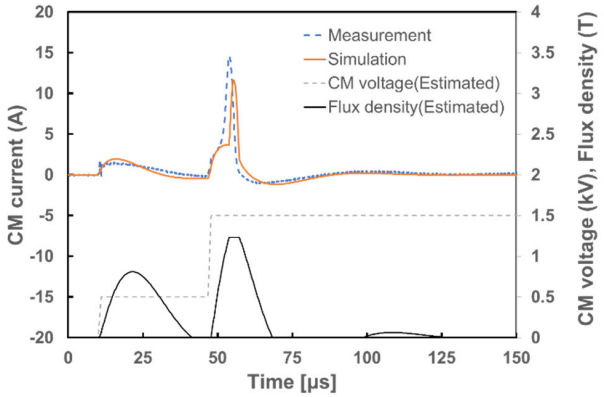

FIGURE 13. Measurement and simulation results (Case V).

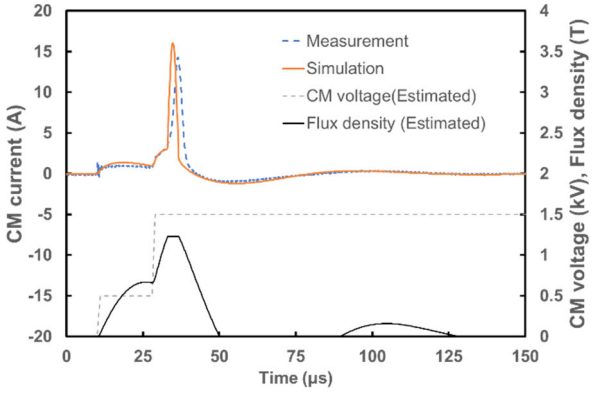

FIGURE 14. Measurement and simulation results (Case VI).

150 μH/n^2 for all simulations. The CM circuit constants for the two parallel motors are based on previous measurements [36], [37].

The saturation behavior of the core is expressed using the limit functions of the LTspice®circuit simulator (Analog Devices, Inc.). The magnetic flux density is calculated by integrating the voltage between both terminals of the CM inductor. The CM voltage is either 500 V or 1000 V based on the measured current waveform. The rise time of the CM voltage is set to 1 μs because the current waveforms do not change even at 10 ns in the simulation. The rise time of the CM voltage does not affect to the simulation circuit [27].

TABLE 3. Comparing B_{max} (T) inside the core.

Numbers& turns	Conventional			Proposed	Result
	Eq. (11)	Eq. (14)	Eq. (18)	Eq. (6)	
Case I $m = 4, n = 1$	2.66	2.72	5.17	1.04	1.23
Case II $m = 7$, n = 1	2.02	2.06	2.96	0.93	1.13
Case III $m = 11, n = 1$	1.61	1.64	1.88	0.84	0.93
Case IV $m = 14, n = 1$	1.43	1.46	1.48	0.79	0.86
Case V $m = 4, n = 2$	5.37	5.44	5.17	1.52	1.23
Case VI $m = 7, n = 2$	4.07	4.12	2.96	1.30	1.23

Note: gray cells are not saturated.

TABLE 4. Minimum number of cores (V_{com} = 1000 V).

turns	Conventional			Proposed	Simulation
	Eq. (11)	Eq. (14)	Eq. (18)	Eq. (6)	
$n = 1$	20	20	17	4	5
$n = 2$	78	79	17	9	9

TABLE 5. Minimum number of cores (V_{com} = 1500 V).

turns	Conventional			Proposed	Simulation
	Eq. (11)	Eq. (14)	Eq. (18)	Eq. (6)	
$n = 1$	44	45	26	13	16
$n = 2$	177	177	26	27	27

Figures 9 through 14 compare the current measurement results in the previous section with the circuit simulation results in this section. In Case V (Fig. 13) and Case VI (Fig. 14), where the current increases rapidly, saturation obviously appears. The simulation results for these cases also show a rapid rise in CM current and the magnetic flux density reaching saturation flux density, indicating that the circuit simulation reproduces the measurement results. In the second impulse of Case I (around 75 μs in Fig. 9), the measured current does not surge, but there is a time when the current increases on the falling edge, which also seems to cause saturation. Simulation results also confirm short-time saturation. In Cases II, III, and IV, the measured and simulated currents are in good agreement. Therefore, it can be concluded that in all test cases, the internal flux density of the core can be properly estimated by circuit simulation.

C. COMPARING METHODS OF CALCULATING NUMBER OF CORES TO PREVENT SATURATION

Table 3 shows the results of the maximum flux density by calculating method in section IIA and IIB for each test cases in Table 1, as well as the flux density estimation results from the simulations. In each calculation, L_1, A_c, R_1, and C_m is the same as those used in the simulations. For the calculations of (11), (14), and (18), R_m is also the same as the values used in the simulations. The results in the calculations (11), (14), and

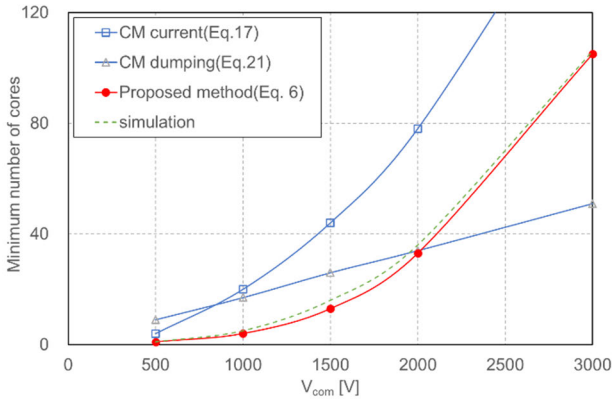

FIGURE 15. Minimum number of cores for preventing saturation ($n = 1$).

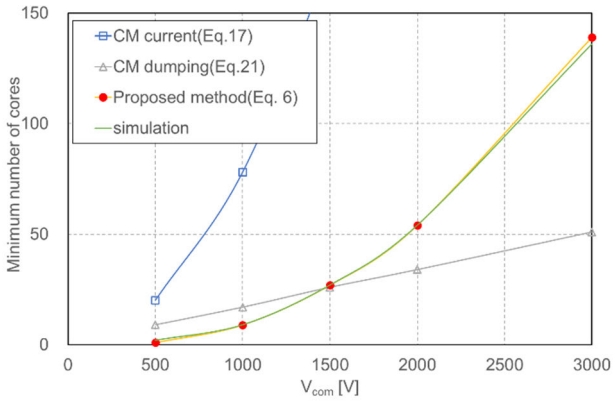

FIGURE 16. Minimum number of cores for preventing saturation ($n = 2$).

(18) are judged to be saturated when they are greater than or equal to B_{sat}, otherwise they are judged to be unsaturated.

As shown in Table 3, results of the conventional method are saturated in all cases while the proposed method in this paper (6), which deviated from the simulation by about 20% with respect to the magnetic flux density in the unsaturated condition, properly determines saturation as the measurement results. Case I (Fig. 9), which determination of saturation differs between (6) and the measurement, is considered to be a boundary condition for saturation, because the CM current in saturation is the same level as the current peak before the saturation. Therefore, we can judge that (6) determines the saturation inside the cores in the CM inductor.

The difference between the magnetic flux density of the proposed method (6) and the measured is due to the fact that method (6) uses only the first stage of the ladder circuit and disregards the CM inductance of the traction motor.

In designing a traction inverter, it is necessary to determine the minimum number of cores that will not saturate based on the given C_{m} and V_{com}. Tables 4 and 5 show the results of determining the minimum number of cores that do not saturate by (11), (14), (18), and (6) for one pulse of CM voltage with $V_{\mathrm{com}} = 1000$ V and $V_{\mathrm{com}} = 1500$ V in Fig. 8. The tables also show the minimum number of cores based on simulation results for comparison.

Tables 4 and 5 also indicate that the proposed method (6) is close to the simulation results. However, the conventional methods, (11), (14) and (17), produce more than twice the number of cores in the simulation. This is because the voltage generated inside the CM inductor is larger than the actual voltage. After all, the flux relaxation inside the core is not taken into account in conventional methods.

In conventional methods, only the results of (18) for $n = 2$ almost equal the simulation results. To verify (6), (14) and (18) in various CM voltages, Figs. 15 ($n = 1$) and 16 ($n = 2$) show the graphs of the minimum number of cores when V_{com} varies from 500 to 3000 V. The V_{com} range consists of the worldwide DC feed voltage based on IEC 60850, and the intermediate voltage of the N700S Shinkansen train [38].

As the voltage V_{com} changes, (14) and (18) deviate far from the simulation results, while (6) remains close to the simulation results over the entire range of CM voltages. Also, as shown in Figs. 15 and 16, V_{com} and the minimum number of cores have an almost quadratic relationship, while (18) shows a proportional relationship. This discrepancy is because that (18) simulates damping condition, whereas the oscillation condition holds for CM inductors in railway traction inverters. These facts indicate that (6) proposed in this paper is useful for estimating the minimum number of cores in the CM inductors of rolling stock traction inverters.

IV. CONCLUSION

This paper proposes a method for estimating the number of nanocrystalline cores to prevent saturation in the design of CM inductors for railway traction inverters without circuit simulation. The proposed method calculates the magnetic flux density from the motor CM capacitance and uses the first stage of the Cauer-type circuit of the core as an equivalent circuit. Comparison with the actual results of CM current measurement using a 1500 V DC inverter for commuter trains shows that the method proposed in this paper adequately represents the occurrence of saturation inside the CM inductor. Furthermore, the minimum number of cores in the range of CM voltages from 500 to 3000 V shows that the proposed method appropriately estimates the minimum number of cores over the entire range of DC input voltages used for railway feed voltage. In contrast, conventional methods in previous studies require more than twice the minimum number of cores through circuit simulation.

ACKNOWLEDGMENT

The authors would like to thank Toshiba Infrastructure Systems Corporation, West Japan Railway Company, and Shigeru Hasumura (formerly of Hitachi Metals Ltd.) for their invaluable cooperation in the measurements.

REFERENCES

[1] A. Ogunsola and A. Mariscotti, *Electromagnetic Compatibility in Railways: Analysis and Management*. Cham, Switzerland: Springer, 2012.
[2] F. R. Holmstrom, D. Turner, and E. Fernald, "Rail transit EMI-EMC," *IEEE Electromagn. Compat. Mag.*, vol. 1, no. 1, pp. 79–82, 1st Quart., 2012.

[3] A. Mariscotti, "Critical review of EMC standards for the measurement of radiated electromagnetic emissions from transit line and rolling stock," *Energies*, vol. 14, no. 3, p. 759, Feb. 2021.
[4] R. Holmes, "Electromagnetic compatibility of electrified railways," in *Proc. Int. Conf. Electr. Railways*, 1995, pp. 131–135.
[5] E. Karadimou and R. Armstrong, "Test of rolling stock electromagnetic compatibility for cross-domain interoperability," *IET Intell. Transp. Syst.*, vol. 10, no. 1, pp. 6–10, 2016.
[6] P. Kirawanich, "An emission management framework for implementing a large railway system with interface complexity," *IEEE Electromagn. Compat. Mag.*, vol. 7, no. 2, pp. 45–53, 2nd Quart., 2018.
[7] C. Place, "Signalling and telecommunication compatibility issues," in *Proc. IET Prof. Develop. Course Electr. Traction Syst.*, 2010, pp. 199–212.
[8] K. Nomura, T. Kojima, and Y. Hattori, "Straightforward modeling of complex permeability for common mode chokes," *IEEJ J. Ind. Appl.*, vol. 7, no. 6, pp. 462–472, 2018.
[9] F. Sixdenier, O. Yade, C. Martin, A. Bréard, and C. Vollaire, "How to include frequency dependent complex permeability into SPICE models to improve EMI filters design?" *AIP Adv.*, vol. 8, no. 5, May 2018, Art. no. 056604.
[10] S. Y. R. Hui, J. G. Zhu, and V. S. Ramsden, "A generalized dynamic circuit model of magnetic cores for low- and high-frequency applications. II. Circuit model formulation and implementation," *IEEE Trans. Power Electron.*, vol. 11, no. 2, pp. 251–259, Mar. 1996.
[11] S. Wang, F. C. Lee, and W. G. Odendaal, "Characterization and parasitic extraction of EMI filters using scattering parameters," *IEEE Trans. Power Electron.*, vol. 20, no. 2, pp. 502–510, Mar. 2005.
[12] M. Kovacic, Z. Hanic, S. Stipetic, S. Krishnamurthy, and D. Zarko, "Analytical wideband model of a common-mode choke," *IEEE Trans. Power Electron.*, vol. 27, no. 7, pp. 3173–3185, Jul. 2012.
[13] I. Stevanovic, S. Skibin, M. Masti, and M. Laitinen, "Behavioral modeling of chokes for EMI simulations in power electronics," *IEEE Trans. Power Electron.*, vol. 28, no. 2, pp. 695–705, Feb. 2013.
[14] S. Takahashi, K. Wada, H. Ayano, S. Ogasawara, and T. Shimizu, "Review of modeling and suppression techniques for electromagnetic interference in power conversion systems," *IEEJ J. Ind. Appl.*, vol. 11, no. 1, pp. 7–19, 2022.
[15] S. Takahashi and S. Maekawa, "Wideband small-signal model of common-mode inductors based on stray capacitance estimation method," *IEEJ J. Ind. Appl.*, vol. 11, no. 3, pp. 514–521, 2022.
[16] A. Muetze, "Scaling issues for common-mode chokes to mitigate ground currents in inverter-based drive systems," *IEEE Trans. Ind. Appl.*, vol. 45, no. 1, pp. 286–294, Jan. 2009.
[17] A. Muetze and C. R. Sullivan, "Simplified design of common-mode chokes for reduction of motor ground currents in inverter drives," *IEEE Trans. Ind. Appl.*, vol. 47, no. 6, pp. 2570–2577, Nov. 2011.
[18] S. Ogasawara and H. Akagi, "Modeling and damping of high-frequency leakage currents in PWM inverter-fed AC motor drive systems," *IEEE Trans. Ind. Appl.*, vol. 32, no. 5, pp. 1105–1114, Sep./Oct. 1996.
[19] W. Tan, C. Cuellar, X. Margueron, and N. Idir, "A high frequency equivalent circuit and parameter extraction procedure for common mode choke in the EMI filter," *IEEE Trans. Power Electron.*, vol. 28, no. 3, pp. 1157–1166, Mar. 2013.
[20] C. Cuellar, N. Idir, and A. Benabou, "High-frequency behavioral ring core inductor model," *IEEE Trans. Power Electron.*, vol. 31, no. 5, pp. 3763–3772, May 2016.
[21] B. Wunsch, S. Skibin, V. Forsstrom, and T. Christen, "Broadband modeling of magnetic components with saturation and hysteresis for circuit simulations of power converters," *IEEE Trans. Magn.*, vol. 54, no. 11, pp. 1–5, Nov. 2018.
[22] B. Wunsch, T. Christen, S. Skibin, and V. Forsstrom, "Broadband circuit model of a ferrite core, including dimensional resonance, saturation, and hysteresis," *IEEE Trans. Magn.*, vol. 55, no. 7, pp. 1–5, Jul. 2019.
[23] G. R. Skutt and F. C. Lee, "Characterization of dimensional effects in ferrite-core magnetic devices," in *Proc. 27th Annu. IEEE Power Electron. Spec. Conf. (PESC)*, vol. 2, Jun. 1996, pp. 1435–1440.
[24] Y. Shindo and O. Noro, "Simple circuit simulation models for eddy current in magnetic sheets and wires," *IEEJ Trans. Fundamentals Mater.*, vol. 134, no. 4, pp. 173–181, 2014.
[25] A. Furuya, Y. Uehara, K. Shimizu, J. Fujisaki, T. Ataka, T. Tanaka, and H. Oshima, "Magnetic field analysis for dimensional resonance in Mn–Zn ferrite toroidal core and comparison with permeability measurement," *IEEE Trans. Magn.*, vol. 53, no. 11, pp. 1–4, Nov. 2017.
[26] A. Ojeda-Rodriguez, C. Dominguez-Palacios, J. Bernal-Mendez, and M. A. Martin-Prats, "Simple and accurate characterization of nanocrystalline common mode chokes," in *Proc. IEEE Int. Symp. Electromagn. Compat. Signal/Power Integrity (EMCSI)*, Aug. 2022, pp. 472–477.
[27] S. Hatsukade, "Circuit simulation for preventing saturation of common-mode chokes in railway traction inverters," in *Proc. 23rd Int. Conf. Electr. Mach. Syst. (ICEMS)*, Hamamatsu, Japan, Nov. 2020, pp. 800–803.
[28] J. Huang and H. Shi, "Suppressing low-frequency components of common-mode voltage through reverse injection in three-phase inverter," *IET Power Electron.*, vol. 7, no. 6, pp. 1644–1653, Jun. 2014.
[29] C. T. Morris, D. Han, and B. Sarlioglu, "Reduction of common mode voltage and conducted EMI through three-phase inverter topology," *IEEE Trans. Power Electron.*, vol. 32, no. 3, pp. 1720–1724, Mar. 2017.
[30] D. Jiang, F. Wang, and J. Xue, "PWM impact on CM noise and AC CM choke for variable-speed motor drives," *IEEE Trans. Ind. Appl.*, vol. 49, no. 2, pp. 963–972, Mar. 2013.
[31] H. Chen, J. Wu, and X. Zheng, "Elimination of common-mode choke saturation caused by self-resonance of the EMI filter in a variable-frequency drive system," *IEEE Trans. Electromagn. Compat.*, vol. 61, no. 4, pp. 1226–1233, Aug. 2019.
[32] R. D. White, "Electrification traction and signalling compatibility," in *Proc. 11th IET Prof. Develop. Course Railway Signalling Control Syst.*, 2006, pp. 132–164.
[33] R. Ford, "IEP EMC hits GWR, LNER and NR," *Mod. Railways*, vol. 75, no. 841, pp. 30–32, 2018.
[34] *IP1 Traction TD1 and Brakes TD5—Phase 2*. Accessed: Jan. 31, 2023. [Online]. Available: https://projects.shift2rail.org/download.aspx?id=3350f0f6-9934-4473-bdb0-8253dcfa493b
[35] R. D. Persichini, D. Di Febo, V. Calà, C. Malta, and A. Orlandi, "EMC analysis of axle counters in the Italian railway network," *IEEE Trans. Electromagn. Compat.*, vol. 57, no. 1, pp. 44–51, Feb. 2015.
[36] A. Yamanaka and S. Hatsukade, "Evaluation of countermeasures of EMI," (in Japanese), *Sym. Railway Cybern.*, vol. 48, p. 510, 2013.
[37] S. Hatsukade, "Extraction of equivalent circuit for motor's common-mode circuit with vector fitting and HLS," in *Proc. Nat. Conv. Rec.*, nos. 5–122, 2015, p. 191.
[38] K. Sato, H. Kato, and T. Fukushima, "Outstanding technical features of traction system in N700S Shinkansen new generation standardized high speed train," *IEEJ J. Ind. Appl.*, vol. 10, no. 4, pp. 402–410, 2021.

SATORU HATSUKADE (Member, IEEE) was born in Tokyo, Japan. He received the B.S. and M.S. degrees in electronics engineering from The University of Tokyo, Japan, in 1994 and 1996, respectively. He is currently pursuing the Ph.D. degree in electrical engineering with Tokyo Metropolitan University, Tokyo.

Since 1996, he has been working with the Railway Technical Research Institute, Tokyo. His current work is in research and development for electromagnetic interference between rolling stock and railway signaling systems. He also consults for electric malfunction of rolling stock and joins in some IEC maintenance teams as an expert.

KEIJI WADA (Senior Member, IEEE) was born in Hokkaido, Japan. He received the Ph.D. degree in electrical engineering from Okayama University, Okayama, Japan, in 2000.

From 2000 to 2006, he was a Research Associate with Tokyo Metropolitan University, Tokyo, Japan, and the Tokyo Institute of Technology. Since 2006, he has been an Associate Professor with Tokyo Metropolitan University. His current research interests include medium-voltage inverter, electromagnetic interference filters, and active power filters.